JOURNAL OF GEOPHYSICAL RESEARCH, VOL. 103, NO. B7, PAGES 15,409–15,422, JULY 10, 1998

The use of high-resolution seismic reflection profiles for fault analysis in the near-shore environment, Weymouth Bay, Dorset, England, United Kingdom

Robert Hunsdale,[1] Jon M. Bull, Justin K. Dix, and David J. Sanderson

Southampton Oceanography Centre, Southampton, England, United Kingdom

Abstract. High-resolution seismic reflection profiles using a Chirp source image a north-south extensional fault set, which cuts rocks of Upper Jurassic age, cropping out on the seafloor of Weymouth Bay, Dorset, England, United Kingdom. The same fault set cuts rocks of similar age along the adjacent coast, and field mapping can be compared directly with the Chirp profiles. Survey lines were shot perpendicular to the fault strike to produce dip sections from which displacements could be measured. One hundred and fifty-three faults were picked on a 15 km line, yielding a fault density of ~ 10 km^{-1}, similar to that measured in the coastal section. Chirp-resolved fault displacements as small as 0.5 m and a maximum fault displacement of 221 m could be inferred from the data. Distribution analysis of offshore fault data indicated that fault displacement is power law with a well constrained exponent of - 0.9. This value is consistent with the power law exponent estimate for fault displacement, over the scale range 2-8 m, onshore. Thus Chirp near-shore seismic reflection profiles can infill a data gap for fault size-frequency relationships that commonly occurs when combining data from outcrops/cores and conventional seismic reflection profiles.

1. Introduction

The realization that the distribution of fault displacement in a region may be power law [*Kakimi*, 1980] opens up the possibility of characterizing fault populations from data sampled over a specific displacement range. Thus a fault displacement distribution measured from either field exposures or commercial seismic reflection surveys may be used to estimate fault densities at any given displacement size beyond the scale limits of the original data set [*Childs et al*, 1990; *Pickering et al.*, 1994]. Such estimates require: (1) the establishment of a power law distribution of the data; (2) the accurate determination of the parameters of the distribution, particularly the power law exponent [*Pickering et al.* 1995], and (3) the testing of the assumption that the same power law relationship applies from the range of the data to that at which the estimate is required. If these conditions apply, application of fractal (power law) concepts allows the estimation of the fracture numbers, the total strain and the degree of reservoir compartmentalization to be made [*Childs et al.*, 1990; *Scholz and Cowie*, 1990; *Walsh et al.*, 1991; *Marratt and Almendinger*, 1991; *Jackson and Sanderson*, 1992; *Yielding et al.*, 1992; *Pickering et al.*, 1994; *Marrett*, 1996].

The fractal (power law) nature of fault displacement has been confirmed from data sets sourced from field exposure and seismic reflection sections. The continuous sampling of faults in field exposures tends to be limited to small displacement sizes, with a typical maximum size of less than a few tens of meters; sample numbers also tend to be small. Seismic reflection profiles, on the other hand, image large faults with a wide range of displacements, generally exceeding about 20 m [*Pickering et al.*, 1994], determined by the resolution of the seismic survey. The number of faults sampled varies according to the amount of seismic section analyzed.

Resolution limitations imposed by these sample collection methods often produce an artificial gap, usually at displacements of ~ 10-20 m, [e.g., *Pickering et al.*, 1994], which may extend from 1 to 20 m where small faults are sampled from drill core [*Yielding et al.*, 1992; *Needham et al.*, 1996]. This size range, below the lower limit of seismic reflection resolution, is important when assessing connectivity and fluid flow in reservoirs. In this paper, high-resolution seismic reflection profiling utilizing Chirp sonar has been used to sample faults with displacements in this critical scale range and to compare the results with field studies of the same fault system.

The faults examined are a conjugate set of north-south trending normal faults within Upper Jurassic and Lower Cretaceous rocks in the Weymouth Bay area, southern England (Figures 1 and 2). These faults are exposed on the seabed, where they were originally mapped by *Donovan and Stride* [1961] using side-scan sonar. A high-resolution seismic reflection survey was undertaken to confirm the nature of Upper Jurassic-Early Cretaceous stratigraphy in the offshore area and thus to accurately determine the location and displacement of the faults.

Similar conjugate north-south striking normal faults are well exposed along a 5.6 km section of the Dorset coast, southern England (Figure 1). Eighty-five faults with displacements in the range 1 cm to 8 m were measured [*Hunsdale and Sanderson*, 1998], and these data will be compared with the seismic data reported here.

2. Background Geology

The Wessex Basin is part of a larger intracratonic basin that covers most of southern England, the English Channel, and parts of

[1]Now at Phillips Petroleum Company, Norway.

Paper number 97JB03675.
0148-0227/98/97JB-03675$09.00

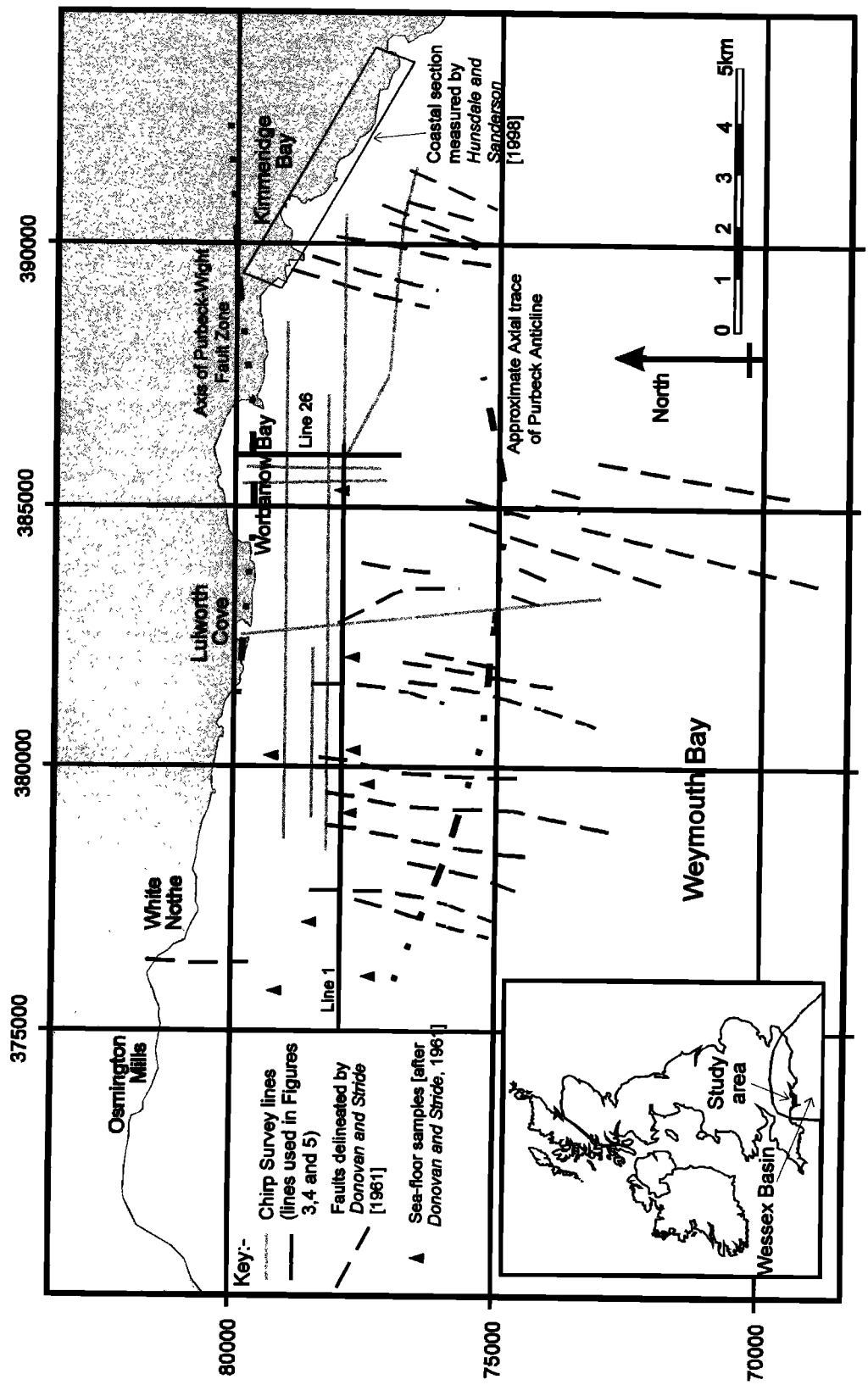

Figure 1. Locality map showing the approximate position of the northern margin of the Wessex Basin (inset). The position of survey lines are marked, as are the seafloor samples and the position of the faults delineated by *Donovan and Stride* [1961]. The position of the Purbeck-Wight Fault Zone and the approximate axial trace of the Purbeck Anticline, the two major structures in the area, are also marked.

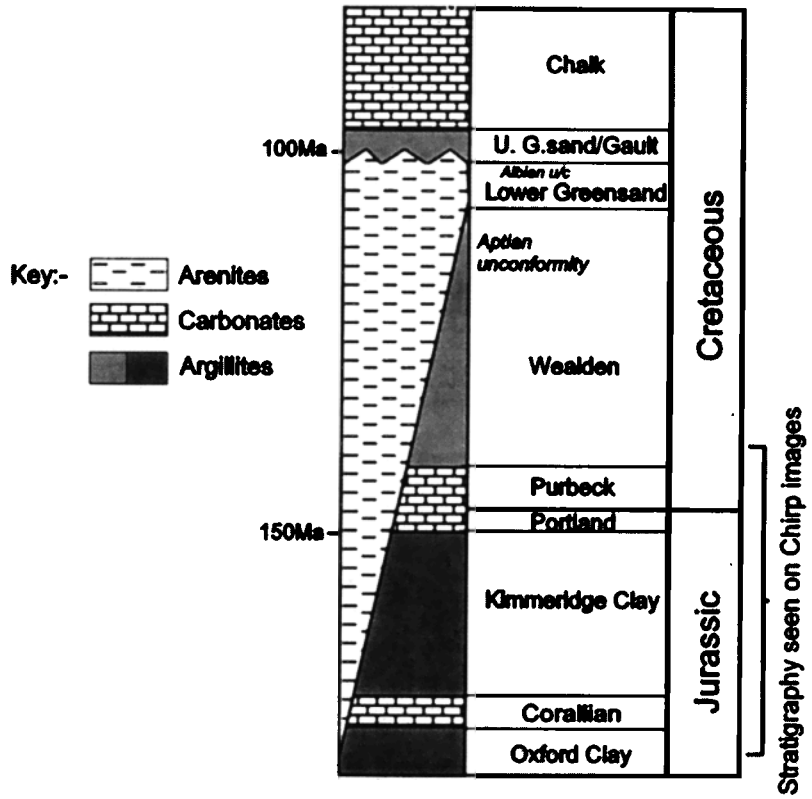

Figure 2. Stratigraphic column showing the Mesozoic and Cainozoic rocks found south of the Purbeck-Wight Fault Zone at the northern margin of the Channel Basin. The part of the stratigraphy seen on Chirp profiles is indicated.

northern France (Figure 1). From Permian times, north-south directed extension reactivated basement structures and led to the development of a series of asymmetric, north and south facing graben and half-graben structures [*Chadwick*, 1985; *Lake and Karner*, 1987; *Karner et al.*, 1987]. Major basin-bounding and intrabasinal growth faults strike east-west, and all major faults dip south. The Mesozoic and Cainozoic stratigraphy seen near the northern margin of the Channel Basin, a subbasin of the Wessex Basin, is presented in Figure 2. The northern margin of the Channel Basin is coincident with both the Purbeck-Wight Fault Zone and the present Dorset coast.

North-south extension culminated in the mid-Cretaceous [*Chadwick*, 1985; *Penn et al.*, 1987; *Karner et al.*, 1987]. Active crustal extension ceased in the Aptian, and the region underwent widespread subsidence. This subsidence is presumed to result from thermal relaxation after the Jurassic and Early Cretaceous crustal rifting events [*Chadwick*, 1993]. Across the Wessex Basin, a thick, flat-lying, postrift sequence of marine sandstones, shales, and chalk built up over the Aptian-Danian period.

From pre-Paleocene times, there is evidence for a change of structural style in the Wessex Basin with the original east-west fabric reactivated as a result of north-south compression [*Curry*, 1965; *Drummond*, 1970; *Chadwick*, 1985; *Penn et al.*, 1987; *Selley and Stoneley*, 1987]. This became more marked during early Tertiary times when, like other basins around southern Britain, the Wessex Basin underwent inversion as a result of north-south compressive stresses associated with alpine movements further to the south [*Ziegler*, 1987; *Coward and Deitrich*, 1989].

Reverse movements on preexisting major, east-west striking, normal faults at depth produced monoclinal and periclinal drape folds in Cretaceous strata at higher tectonic levels. Fault movements exposed Middle to Upper Jurassic strata in anticlinal structures south of the Purbeck- Wight Fault Zones [*Donovan and Stride*, 1961; *House*, 1961]. These rocks have been exhumed from depths of between 2 and 2.5 km [*Bray et al.*, 1998]. In Weymouth Bay the doubly plunging Purbeck Anticline is cored by rocks of Corallian and Oxford Clay age [*Donovan and Stride*, 1961]. Dips increase from the core of the anticline shoreward, reaching an average of 35°N before steepening to vertical and becoming overturned close to the Purbeck-Wight Fault [*Donovan and Stride*, 1961; *House*, 1989]. A complete stratigraphic section of Corallian to Wealden rocks crop out along the seabed. Faulting along the coast is at a low oblique angle to the stratigraphic grain and precludes analysis of such a thick stratigraphic sequence through a single continuous section.

The last phase of tectonism took place in the Oligocene-Miocene and is represented by a conjugate, north-south striking extensional fault set [*Hunsdale and Sanderson*, 1998]. These are well developed along the Dorset coast and in the adjacent near-shore area (Figure 1) [*Donovan and Stride*, 1961]. It is this last stage of faulting that is the main subject of the analysis in this paper.

3. Data Acquisition and Processing

Knowledge of both fault and stratigraphic trends from the onshore and offshore areas aided survey design [*Donovan and Stride*, 1961]. By running offshore survey lines in an east-west direction perpendicular to mean fault strike (Figure 1), orientational bias is negated, and true fault dip and displacement are represented on Chirp profiles. Collection of fault data in the onshore area was carried out using a scanline technique [*La Pointe and Hudson*, 1985] and applying a Terzaghi correction to compensate orientational bias [*Hunsdale and Sanderson*, 1998; after *Peacock*

and Sanderson, 1994] . Offshore seismic lines were also acquired in a north-south direction (Figure 1) to link the main east-west lines and to allow the geology on coast-parallel lines to be tied directly to that onshore. Navigation was controlled by employing a differential global positioning system (DGPS).

Data were acquired using Chirp sonar, a digital, frequency-modulated, subbottom profiler designed to obtain marine high-resolution seismic reflection data. Chirp systems utilize a wideband sonar which produces frequency modulated (FM) pulses that linearly sweep a range of frequencies. The key feature of Chirp systems is that the source signature is known and can be correlated or "match-filtered" with the data recorded by the hydrophone. The correlated data can then be processed using conventional seismic reflection algorithms. The full processing sequence for the data shown in this paper is correlation, true amplitude recovery (using a water column velocity of 1480 ms^{-1} and a sediment velocity of 2700 ms^{-1}), F-X deconvolution, and F-K Stolt Migration.

When calculating depth and thickness measurements on Chirp profiles an average velocity of 2700 ms^{-1} was assumed for the compacted Upper Jurassic sediments. For the 2-8 kHz swept source used here the central or carrier frequency is 4.6 kHz, yielding a theoretical resolution (Rayleigh criterion) of 0.147 m for the typical rock velocities of 2700 ms^{-1} encountered. In practice, the effective resolution of the final migrated seismic reflection data from which structural measurements were made is much lower, and we estimate that the practical vertical resolution is ~ 0.5 m.

The Chirp trace spacing during the survey was 0.6 m on average. This spacing is smaller than the minimum required to ensure that the greatest possible horizontal resolution was achieved. In this paper the key measurements that are made are the vertical separation of stratigraphy across faults which strike perpendicular to the survey line. It is possible that closely spaced faults will appear as a single fault, and for the typical depth ranges in Weymouth Bay, faults more closely spaced than 2 m are unlikely to be imaged separately.

4. Interpretation of Chirp Profiles

Donovan and Stride [1961] undertook a side-scan sonar and "asdic" echo-ranging survey of Weymouth Bay. During their work, rock samples were gathered and dips were measured from rock ledges which cropped out on the seabed. Samples close to lines surveyed in this study have been used to aid interpretation (Figure 1). Offshore dip measurements recorded in *Donovan and Stride* [1961] were also used to aid estimates of true bed thickness.

Formations in the Upper Jurassic and lowest Early Cretaceous sequence in southern England comprise a series of shallow marine clays, sandstones, and limestones (Corallian), deeper offshore muds with aerially extensive diagenetic carbonate layers and coccolithic limestone marker beds (Kimmeridge Clay), and marginal marine to continental limestones, evaporites, and carbonate-rich sands (Portland and Purbeck). South of the Purbeck-Wight Fault Zone in the northern part of the Channel Basin, these sediments have a measured thickness of 728 m (Table 1) [*Arkell*, 1947; *Talbot*, 1973; *Cox and Gallois*, 1981; *El-Shahat and West*, 1981; *House*, 1989]. Accurate recognition of formations and, on a finer scale, marker beds within them are needed to calculate fault displacement. *Arkell* [1935, 1936, 1947] laid the groundwork for detailed stratigraphic and sedimentological studies on the Corallian [*Wilson*, 1968; *Talbot*, 1973, *Sun*, 1990], Kimmeridge Clay [Cox and Gallois, 1981], Portland [*Townson*, 1975] and Purbeck Formations [*El-Shahat and West*, 1981; *Ensom*, 1985]. From these studies accurate thickness measurements for each formation can be obtained (Table 1).

Table 1. Comparison of Measured Thicknesses With Estimated Thicknesses From Chirp Line 26

Stratigraphy		Measured Thickness, m	Estimated Thickness From Chirp, m	Reflection Characteristics and Seabed Topography
Cretaceous	Wealden	not calculated	not calculated	
	Purbeck			closely spaced reflectors: elevated seabed, craggy topography
	Durlston	29	25	
Upper Jurassic	Portland			
	Lulworth	50	51	
	Portland Stone/Sand	68	65	spaced strong reflectors with many more faint reflecting horizons, full stratagraphic correlation: seabed gentle but stepped across strong reflectors
	Kimmeridge Clay			
	Upper	120	119	
	Middle	116	101	
	Lower	258	373	
	Corallian	87	87	very strong reflectors, distinctive patterns can be used to identify individual units: seabed generally smooth, stepped where strong reflectors are more steeply dipping
	Oxford Clay	not calculated	not calculated	
Total Thickness		728	821	

The measured thicknesses are after *Talbot* [1973], *Cox and Gallois* [1981], *Ensom* [1985], *House* [1989], and *Sun* [1990]. Estimated thicknesses were calculated by using horizontal distance down true dip and dip angles measured on the adjacent coast and on subsea ledges [after *Donovan and Stride*, 1961]. A strong correlation exists except for the Lower Kimmeridge Clay, which is estimated to be 117 m thicker offshore than in onshore boreholes or coastal exposure (see text for discussion). The seafloor topography and reflection characteristics for each unit are also given.

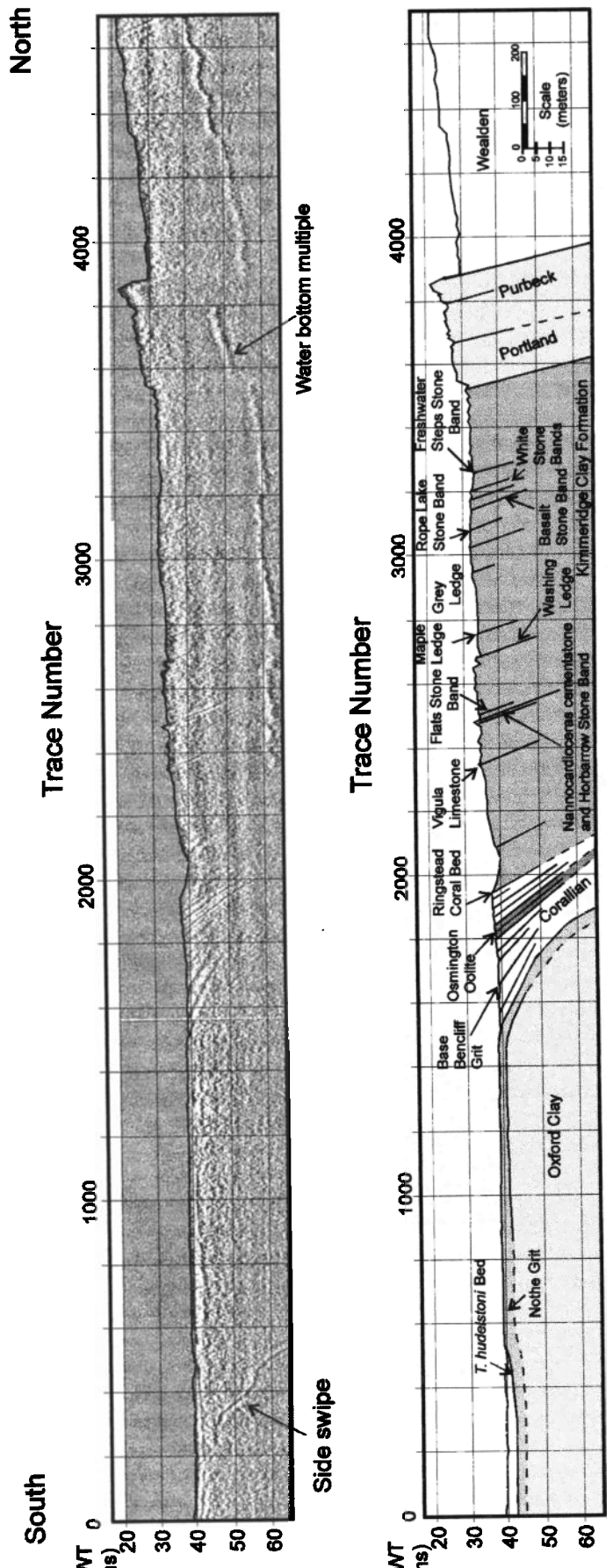

Figure 3. Seismic image and interpreted section for line 26, which runs north into Worbarrow Bay. Lines in this orientation allow east-west orientated survey lines to be tied into the onshore geology. The prominent topographic high in the seabed (trace numbers 3500 - 3900) represents the limestones of the Portland and Purbeck formations. South of this, prominent reflectors can be correlated with carbonate layers in the Kimmeridge Clay. The distinctive closely spaced reflectors of the Corallian can be seen between trace numbers 1600 and 2000 with the Nothe Grit defining a fold whose axial trace is around trace number 1200. The asymmetry of the fold is largely apparent, as the fold plunges to the northeast, thus the survey line is oblique to the axial trend. Marker beds used in estimating displacement values are marked on the interpreted section.

To assess the response of Chirp sonar to these formations, a series of survey lines were orientated down stratigraphic dip in a north-south direction into Worbarrow Bay (Figure 1). The processed Chirp profile for one such north-south line, line 26, is presented in Figure 3 along with an interpreted section. Chirp profile estimates of formation thickness, reflection characteristics, and seabed topography are given in Table 1. Onshore formation dip data from the Purbeck, Portland, and Upper Kimmeridge Clay and from offshore Lower Kimmeridge Clay [*Donovan and Stride*, 1961] were used to validate the attitude of post-migrated reflectors on Chirp profiles.

Interpretation of line 26 is centered on the elevation in seabed topography caused by the relatively resistant limestones of the Purbeck and Portland Formations (trace numbers 3,550-3,900 in Figure 3). Worbarrow Bay (Figure 1) forms a crescent embayment with Purbeck and Portland limestones forming rock promontories into the bay, behind which the Wealden Clay has been eroded out. When the strike and dip from onshore Purbeck/Portland outcrops are projected across the concave southward dipping bay floor, good correlation is found with the DGPS coordinates of the elevated ridge in the bay.

Interpretation southward through the Kimmeridge Clay and Corallian Formations is facilitated by a series of intra-formational reflectors on the Chirp profiles. The occurrence of thin (0.5-2 m) laterally persistent dolomitic cementstone and coccolithic limestone marker beds in the Kimmeridge Clay Formation allows the accurate correlation of Chirp profiles with the measured stratigraphic thickness of *Cox and Gallois* [1981]. Those beds used in defining stratigraphy and in establishing fault displacement data are shown in Figure 4.

From Table 1 it can be seen that there is excellent correlation between the actual measured onshore thickness of the Upper Jurassic and Early Cretaceous Formations and those estimated from the processed Chirp profiles, except that the Lower Kimmeridge Clay is ~ 120 m thicker on the Chirp profile (Figure 3). There are two possible explanations for this. First, the apparent thickening in the offshore area could result from the Upper Jurassic palaeocoastline being oblique to the current coastline [*Wilson*, 1967, *Talbot*, 1974] that is controlled by later tectonic events [*House*, 1989]. Second, the overthickening in the offshore area could represent syn-depositional extension on the Purbeck-Wight Fault during Lower Kimmeridge times. Further discussion is beyond the scope of available data.

An example of the quality and detail that can be produced by Chirp sonar is shown in Figure 4. Here a section of 1,000 traces through the Corallian Formation near the start of line 1 (Figure 1) is shown. Being orientated east-west, the line is parallel to the regional strike of the bedding [*Donovan and Stride*, 1961]. However, when depth converted, the reflectors show a gentle dip (»7°) to the west, which may relate to folding around the flanks of the Purbeck Anticline or to tilting associated with late north-south extensional faulting. The latter explanation is favored here since a

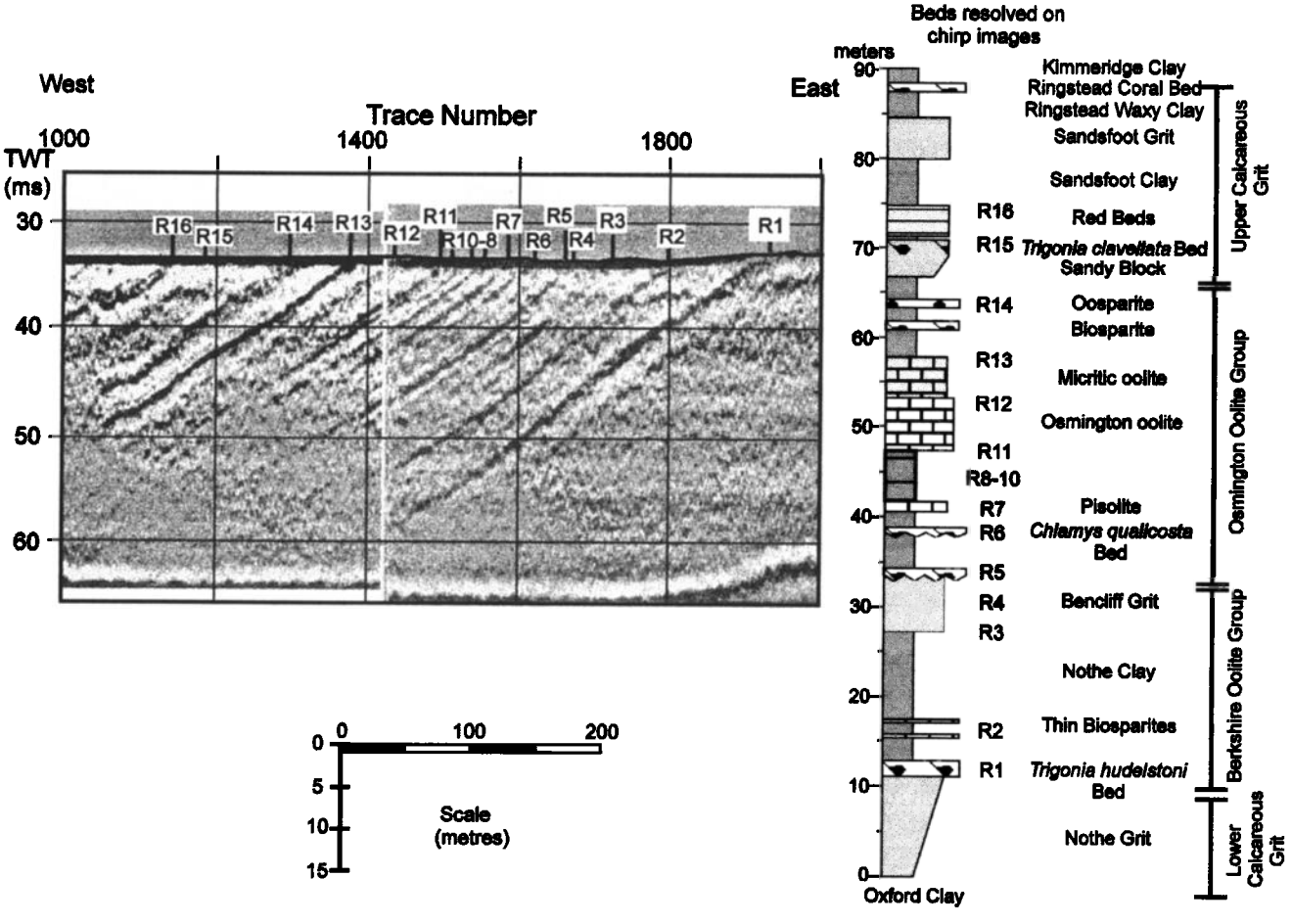

Figure 4. Seismic image of 1000 trace section of line 1 showing the detailed stratigraphy of the Corallian. Sedimentary column after *Talbot* [1973], *House* [1989] and *Sun* [1990]. The sixteen reflectors identified on the seismic image relate dominantly to the tops of carbonate and grit units within the predominantly shaley sequence, although the bases of some of the thicker units (R3 and R11) are also identified.

large normal fault can be seen on the western side of the section (Figure 5).

Several studies have produced detailed sedimentological and stratigraphic information for these rocks [*Arkell*, 1936; *Wilson*, 1968; *Talbot*, 1973; *Sun*, 1990]. A combination of *Talbot*'s [1973] and *Sun*'s [1990] sedimentary and stratigraphic sequences are presented in Figure 4 for comparison with the Chirp profile. A good correlation can be made between the Chirp profile and *Talbot*'s [1973] measured stratigraphy from the *Trigonia hudelstoni* bed to the top of the red beds (R1 and R16 in Figure 4 and Table 2). Clearly the combination of bed thickness, together with the acoustic impedance contrast between clays and coarser limestones and sandstones in the Corallian, provide ideal conditions for high-resolution seismic acquisition. Given these conditions, submeter scale stratigraphic detail can be resolved with limestones as thin as 0.2 m recognised in clay units. Sixteen reflectors are identified (Figure 4), which can correlated with Corallian beds exposed along the coast at Osmington Mills (Figure 1).

The coarse, rubbly, fossil lag deposits (R1, *Trigonia hudelstoni* bed; R5, top Bencliff Grit; and R16, Ringstead Coral bed) form strong reflectors which can be used to correlate across faults. Similarly, the sharp contrast seen at limestone-clay interfaces (R13, top Micritic Oolite) provides equally strong reflectors. *Sun* [1990] provides a more detailed sedimentological description of the clay-rich member between the Osmington Oolite and the Bencliff Grit (Figure 4), which he refers to as the Upton Member [after *Wright*, 1986]. *Sun* [1990] defines an interbedded sequence of calcareous clays and nodular and bioclastic limestone. Such lamination would account for reflectors R6-R10 seen in Figure 4.

Being able to resolve stratigraphy in such fine detail allows the recognition of small fault displacements. Figure 5 shows a section of a Chirp profile from an east-west orientated 15 km survey line (line 1) which transects the northern limb of the Purbeck Anticline (Figure 1). One hundred and fifty-three faults with displacements ranging from 0.5-221 m (Table 3) were identified. In the same area, *Donovan and Stride* [1961] identified only 9 faults, for which only relative displacement information could be obtained (Figure 1). Faults imaged here have a density of ~ 10 km^{-1} and show bimodal conjugate dips (range of 42°-70°; average dip of 57°). The same characteristics are shown by faults of similar orientation which crop out along the adjacent coastal section [*Hunsdale and Sanderson*, 1998].

Figure 5 shows that north-south striking faulting clearly post-dates the formation of the doubly plunging anticline. The Upper Jurassic strata plunge to the west between trace numbers 0 and 8,000 and to the east from trace 8,000 onward. The eastward portion of the line is complicated by faulting and the intersection of folds, for example, around trace number 15,000. Correlation of this fold with a similar feature on a parallel line 250 m to the north indicates that these folds plunge to the northeast. Faulting is not evenly distributed along the line with zones of intense faulting being interspersed with areas of relatively few faults (Figure 5). Fault recognition is also easier in the Corallian and parts of the Kimmeridge Formations where closely spaced marker beds can be identified and allow accurate displacements to be determined (trace numbers 14,200-15,200 and 17,000-17600, respectively in Figure 5). Fault identification in the more homogenous clay-rich portions of the stratigraphy is more difficult, but the juxtaposition of these with the layered Corallian across large displacement faults produces spectacular images (trace numbers 11,000-12,000 in Figure 5).

Table 2. Comparison of Measured Thickness for the Corallian With Estimated Thickness From Line 1

Units Within Corallian	Thickness to Unit Top, m	Reflection Events on Chirp Profile	Measured Distance to Unit Top, m	Estimated Distance to Unit Top From Chirp Profiles, m
Ringstead Coral bed	88			
Ringstead Waxy Clay	87.5			
Sandsfoot Grit	84			
Sandsfoot Clay	80			
Red bed	74	top red bed (R16)	61.5	60
Trigonia clavellata and Sandy Block	71	top *T.clavellata* bed (R15)	58.5	57
Clay with Oosparite layer	66.5	top Oosparite (R14)	51	50
Micritic Oolite	57.5	top Micritic Oolite (R13)	45	43.5
Osmington Oolite	53	top Osmington Oolite (R12)	40.5	39.5
		base Osmington Oolite (R11)	34.5	34
Clays with pisolite and *Chlamys qualicosta* bed	47	Calcareous layers in clay (R8-10)		
		top pisolite (R7)	27.5	28
		top *C.qualicosta* bed (R6)	25.5	26
Bencliff Grit	34	top Bencliff Grit (R5)	21.5	22
		internal surface (R4)		
		base Bencliff Grit (R3)	14.5	16
Nothe Clay with thin biosparites near base	27	upper Biosparite (R2)	5	6
Trigonia hudelstoni bed	12.5	top *T.hudelstoni* bed (R1)	0	0
Nothe Grit	10			
Oxford Clay	0			

Measured thicknesses are after *Talbot* [1973] and *Sun* [1990]. See trace numbers 1000-4000 in Figure 4. Reflectors on the high-resolution sesmic image can be matched perfectly with the sedimentological units from the onshore Corallian, with beds as thin as 0.2 m imaged, and fault displacements can be accurately picked.

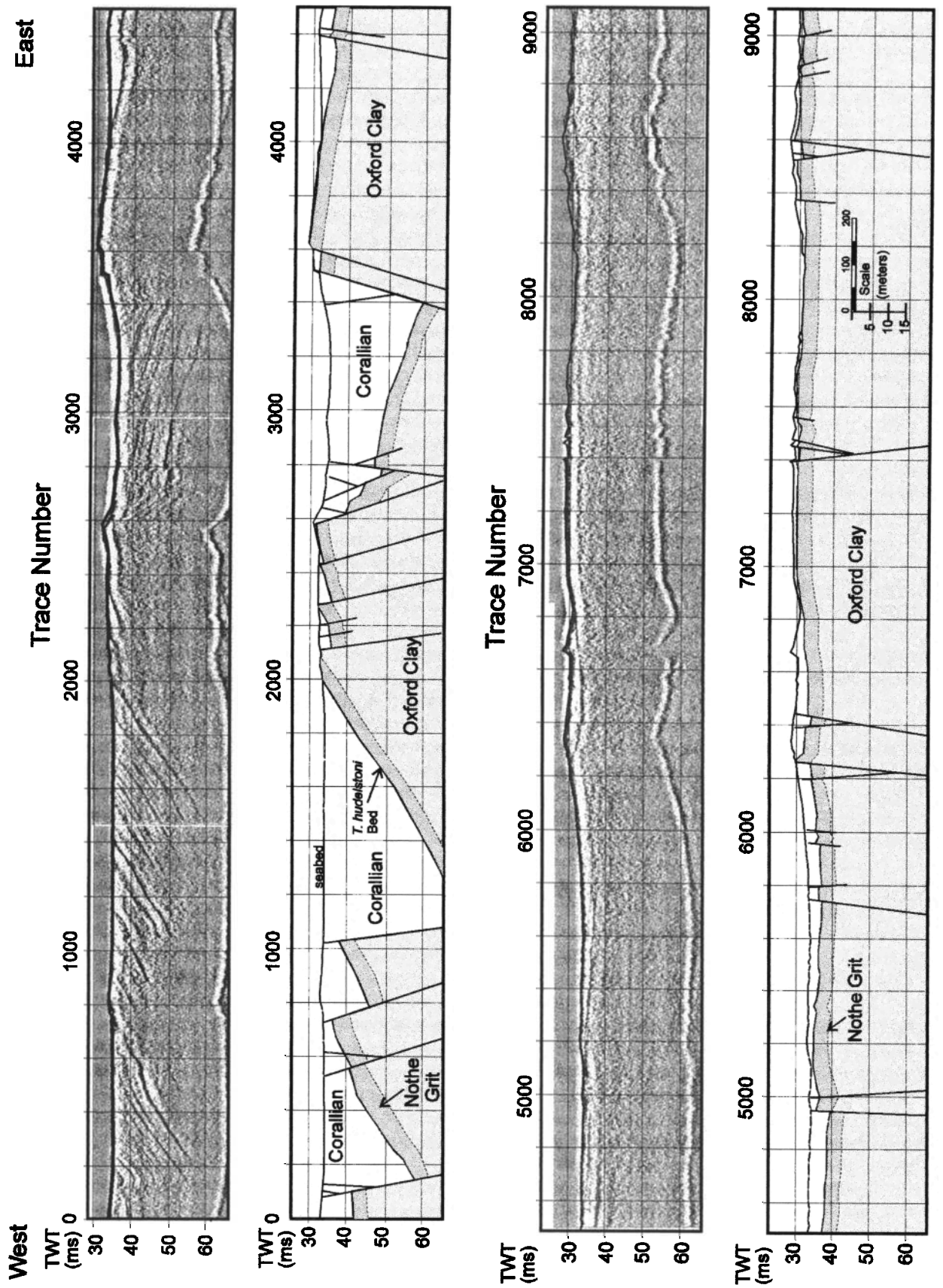

Figure 5. Seismic image and interpreted section for line 1. Faulting is most evident in Corallian areas but harder to pick in rocks that are dominantly clay. The line runs parallel to the axis of the doubly plunging Purbeck anticline and the Oxford Clay can be seen in the core of the structure (trace numbers 4000 - 9000). East of this, faulting becomes intense, and minor folds can be seen, Extrapolation between adjacent lines suggest's that minor folds plunge northeast. One hundred and fifty-three faults were picked on this line.

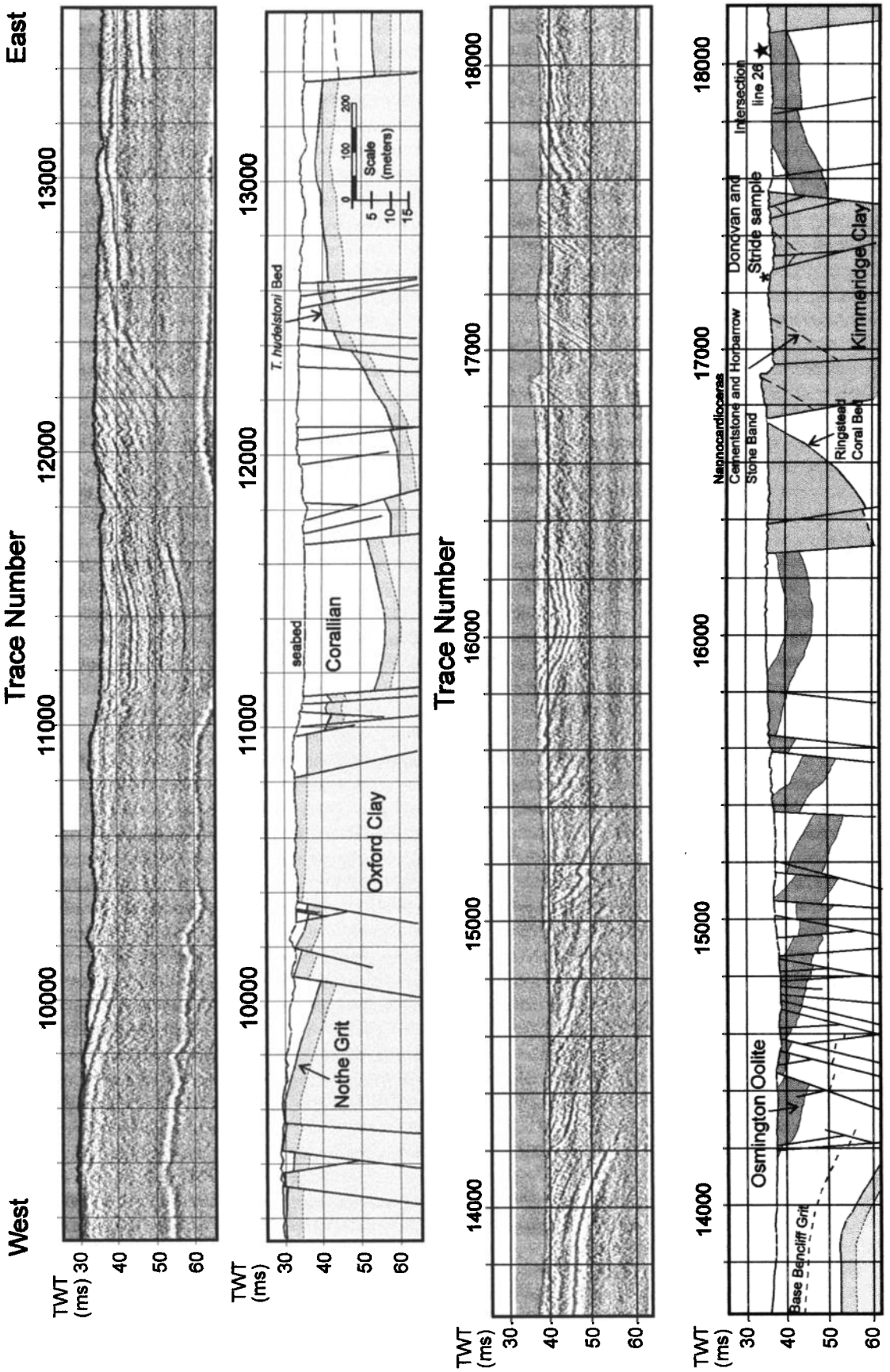

Figure 5. (continued)

Table 3. Spacing, Throw, and Dip Data for Faults Resolved on Line 1

Fault	Distance, m	Throw, ms	Throw, m	Dip Angle	Dip Direction
1	50,4	0,8	1,08	50	East
2	58,8	1,6	2,16	54	East
3	77,7	10,8	14,58	61	East
4	373,8	0,8	1,08	52	East
5	409,5	0,4	0,54	65	West
6	466,2	11,6	15,66	58	East
7	684,6	38,4	51,84	64	East
8	1335,6	4,4	5,94	49	East
9	1367,1	1,6	2,16	48	East
10	1398,6	0,4	0,54	48	East
11	1444,8	4,8	6,48	46	East
12	1587,6	2	2,7	52	East
13	1709,4	1,2	1,62	42	East
14	1753,5	20	27	65	West
15	1785	2,4	3,24	52	East
16	1801,8	1,6	2,16	50	West
17	1827	1,2	1,62	51	West
18	1831,2	0,4	0,54	56	East
19	2209,2	1,2	1,62	59	West
20	2221,8	0,8	1,08	65	West
21	2242,8	31,2	42,12	61	West
22	2293.2	1,6	2,16	60	West
23	2809,8	2	2,7	60	West
24	2826,6	1,2	1,62	61	West
25	3204,6	5,6	7,56	58	West
26	3385,2	4	5,4	59	East
27	3704,4	1,2	1,62	62	West
28	3750,6	4,8	6,48	58	East
29	3826,2	1,6	2,16	63	West
30	3868,2	0,8	1,08	69	West
31	4011	0,8	1,08	68	East
32	4027,8	3,6	4,86	54	West
33	4128,6	0,8	1,08	58	East
34	4141,2	0,4	0,54	60	West
35	4767	1,2	1,62	57	East
36	4783,8	0,8	1,08	51	West
37	4813,2	0,8	1,08	54	West
38	4838,4	0,4	0,54	54	West
39	5346,6	10	13,5	56	West
40	5422,2	1,6	2,16	52	West
41	5535,6	2,4	3,24	51	East
42	5552,4	0,4	0,54	48	East
43	5560,8	3,2	4,32	48	West
44	5607	4	5,4	46	East
45	5632,2	4,8	6,48	54	West
46	5737,2	0,8	1,08	50	East
47	5791,8	1,6	2,16	50	East
48	5829,6	1,2	1,62	50	East
49	5976,6	1,2	1,62	50	West
50	6052,2	6	8,1	48	East
51	6064,8	4,8	6,48	50	West
52	6153	1,2	1,62	50	West
53	6501,6	7,2	9,72	52	West
54	6547,8	2	2,7	51	West
55	6652,8	0,4	0,54	46	East
56	6657	1,2	1,62	48	West
57	6678	0,8	1,08	48	East
58	6686,4	3,2	4,32	46	West
59	6993	11,2	15,12	48	East
60	7098	1,2	1,62	50	East
61	7123,2	2,8	3,78	49	East
62	7140	2	2,7	52	West
63	7156,8	1,6	2,16	54	East
64	7173,6	13,2	17,82	54	East
65	7513,8	4,8	6,48	58	East
66	7560	2,8	3,78	52	East

Table 3. (continued)

Fault	Distance, m	Throw, ms	Throw, m	Dip Angle	Dip Direction
67	7585,2	2,4	3,24	54	East
68	7614,6	0,8	1,08	47	West
69	7694,4	6,4	8,64	50	East
70	7774,2	6	8,1	55	East
71	7791	0,8	1,08	70	West
72	7963,2	1,2	1,62	62	West
73	7980	2	2,7	60	West
74	8026,2	1,6	2,16	59	West
75	8093,4	0,4	0,54	58	West
76	8114,4	0,8	1,08	56	East
77	8143,8	13,6	18,36	62	East
78	8614,2	8	10,8	63	East
79	9118,2	1,6	2,16	46	East
80	9147,6	6	8,1	48	East
81	9198	0,8	1,08	50	West
82	9261	0,4	0,54	45	East
83	9303	7,6	10,26	46	West
84	9332,4	0,4	0,54	49	East
85	9357,6	0,8	1,08	51	West
86	9387	3,6	4,86	51	West
87	9395,4	1,2	1,62	50	East
88	9399,6	1,2	1,62	52	East
89	9429	0,8	1,08	50	West
90	9450	0,4	0,54	51	West
91	9513	0,8	1,08	52	West
92	9534	0,8	1,08	46	East
93	9550,8	0,4	0,54	56	East
94	9571,8	1,2	1,62	55	West
95	9584,4	0,8	1,08	52	East
96	9622,2	0,8	1,08	54	West
97	9630,6	0,4	0,54	48	East
98	9664,2	1,6	2,16	55	West
99	9706,2	4	5,4	59	West
100	9748,2	0,4	0,54	58	East
101	9765	3,2	4,32	54	West
102	9874,2	17,2	23,22	60	West
103	10017	12,8	17,28	60	West
104	10054,8	2	2,7	61	West
105	10151,4	2,8	3,78	62	West
106	10449,6	57.6	77,76	52	East
107	10836	164	221	54	East
108	11092,2	23,6	31,86	49	East
109	11209,8	6,4	8,64	47	East
110	11239,2	3,2	4,32	47	East
111	11260,2	158	214	48	West
112	11281,2	3,2	4,32	53	East
113	11461,8	2,8	3,78	48	East
114	11659,2	58	78,5	49	East
115	11793,6	1,6	2,16	48	East
116	11806,2	1,2	1,62	50	East
117	11928	15,2	20,52	56	East
118	12314,4	0,4	0,54	54	East
119	12377,4	0,8	1,08	55	East
120	12398,4	0,4	0,54	51	West
121	12583,2	1,2	1,62	58	East
122	12608,4	0,8	1,08	56	East
123	12637,8	0,8	1,08	59	East
124	12667,2	0,4	0,54	57	West
125	12776,4	2,4	3,24	59	West
126	12847,8	4,4	5,94	59	West
127	12965,4	2,4	3,24	51	East
128	12978	0,8	1,08	55	West
129	12994,8	0,4	0,54	55	West
130	13049,4	1,2	1,62	56	West
131	13070,4	1,2	1,62	56	West
132	13083	2,8	3,78	56	West
133	13280,4	0,4	0,54	51	East

Table 3. (continued)

Fault	Distance, m	Throw, ms	Throw, m	Dip Angle	Dip Direction
134	13293	0,4	0,54	52	West
135	13326,6	1,2	1,62	52	West
136	13368,6	0,8	1,08	52	West
137	13822,2	0,8	1,08	60	West
138	13897,8	0,4	0,54	59	East
140	13923	2,4	3,24	56	West
141	13939,8	0,4	0,54	48	West
142	14023,8	2	2,7	52	West
143	14049	4	5,4	53	West
144	14267,4	0,8	1,08	56	West
145	14330,4	7,2	9,72	62	West
146	14439,6	1,2	1,62	51	West
147	14574	1,6	2,16	53	West
148	14599,2	10,4	14,04	53	West
149	14716,8	7,6	10,26	49	West
150	15535,8	1,6	2,16	56	West
151	15565,2	2,4	3,24	56	West
152	15590,4	1,6	2,16	57	West
153	15653,4	1,2	1,62	54	East

Throws are picked in milliseconds and depth converted using a velocity of 2700 ms^{-1}. Fault dip angles are measured directly on the time-migrated profiles and corrected to allow for vertical exaggeration. One hundred and fifty-three faults were picked over a displacement range of 0.54-221 m.

5. Fractal Analysis of Fault Displacement Data

Many fault characteristics such as displacement [*Kakimi*, 1980; *Childs et al.*, 1990; *Jackson and Sanderson*, 1992; *Yielding et al.*, 1992; *Pickering et al.*, 1994, 1995; *Needham et al.*, 1996; *Hunsdale and Sanderson*, 1998] follow a power law distribution. A power law distribution can be defined by:

$$N = c\,U^{-D} \quad (1)$$

or

$$\log N = \log c - D \log U \quad (2)$$

where N is the number of objects with size [3] U, D is the power law exponent of the distribution, and c is a constant. Unlike other distribution models, a power law theoretically extends over an unlimited scale range. As a result, a sample from a population that conforms to a power law distribution at one scale can be used to predict the number of similar features at different scales.

The most common method of representing data sets which conform to a power law distribution are log-scale, cumulative frequency graphs (Figures 6a and 7a). Power law distributions should form a straight line trace, the slope of which is the power law exponent (D value) of the distribution. Natural data sets are, however, scale-limited beacause of the resolution limits of the data acquisition methods. This results in the divergence of the data from the underlying power law distribution at both the small and large size limits of a data-set [*Pickering et al.*, 1995]. Both phenomena are displayed by the data presented in Figure 6a. *Pickering et al.* [1995] showed that on log-scale cumulative frequency distribution plots, truncation at the lower size limit will not affect the determination the D value of the power law distribution if the truncated part of the data set is excluded in slope-fitting calculations. However, the upper size limit causes convex upward curvature of the log-log plot and an over-estimation of D. In addressing this problem *Pickering et al.* [1995] showed that other graphing techniques were less susceptible to these finite range effects and give more accurate estimates of D. One of these, the log-interval graph is used here to confirm D value estimates from log-scale cumulative frequency plots (Figures 6b, 7b and 8). The log-interval graph plots the frequency in equal class intervals of log (displacement) and avoids the need for any assumptions about data beyond the scale range of the data, when calculating D (see *Pickering et al.* [1995] for full discussion). A log-class interval of 0.1 was used for the log-interval graphs. Linefitting was carried out

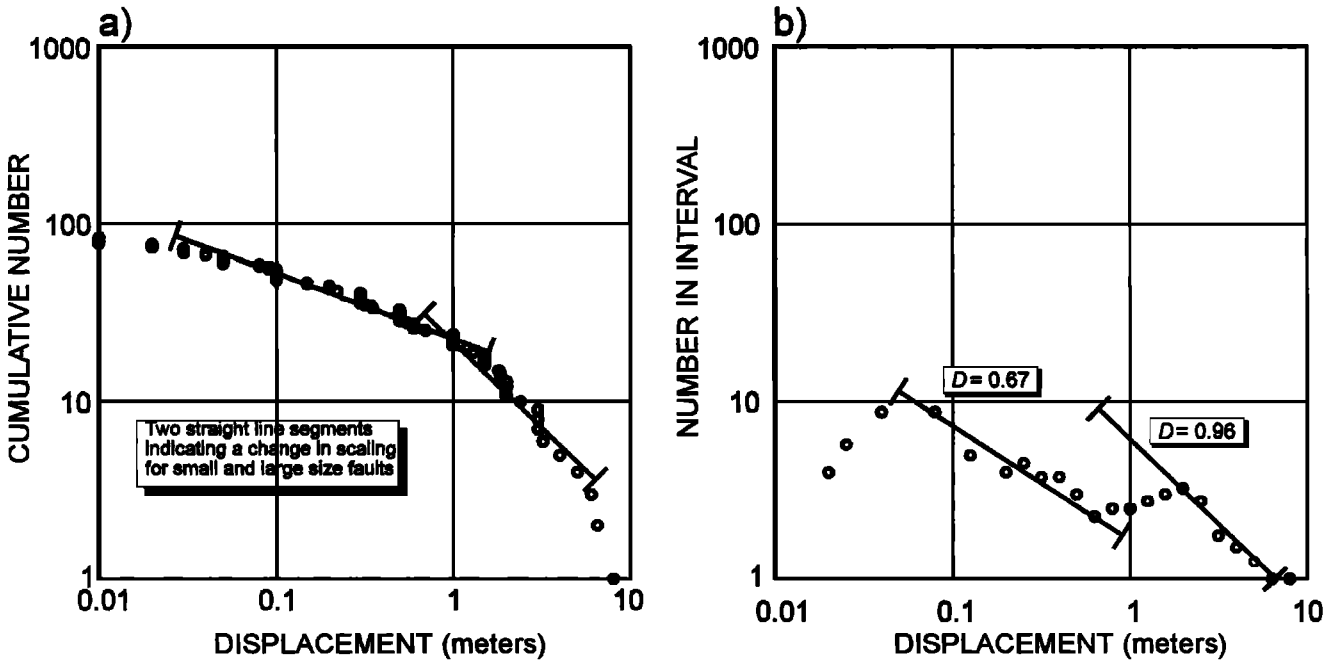

Figure 6. (a) Cumulative frequency graph and (b) log-interval graph defining the change in fault size scaling at throws of between 1 and 2 m for the onshore data. The cumulative frequency graph also illustrates the deviations commonly seen at the small (truncation) and large scale limits (finite range effect) of natural data sets [*Pickering et al.*, 1995]. The log-interval graph shows that the fault throws in the scale range 2 - 8 m have a D value of 0.96, which is significantly higher than the D value of 0.67 for fault throws over the range 5 - 80 mm.

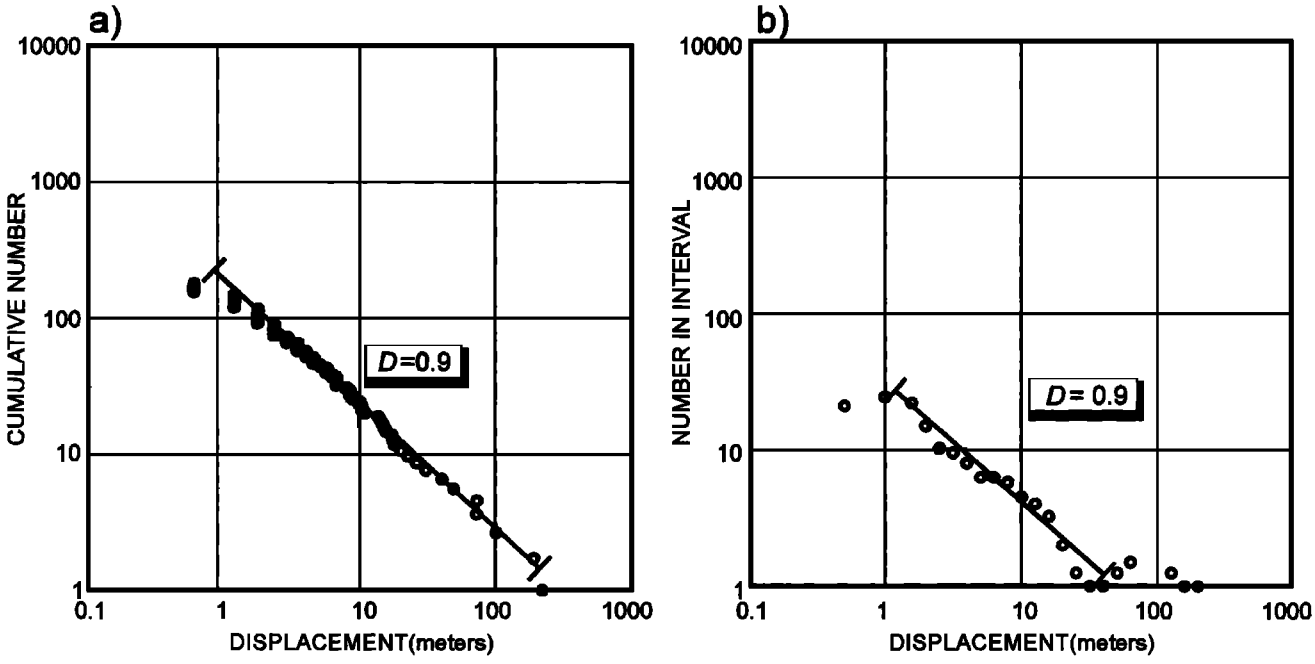

Figure 7 (a) Cumulative frequency graph and (b) log-interval graph showing that fault throws measured offshore are power law and are characterized by a D value of 0.90. Truncation, below 1 m, can be seen on the cumulative frequency graph, suggesting that all faults above 1 m on this image have been resolved.

using a weighted least -squares algorithm [*Press et al.*, 1986; *Pickering et al.*, 1994] on both graph types.

Pickering et al. [1995] used a Monte Carlo simulation of the sampling and analysis process to show that confidence limits on D value estimates are inversely proportional to the square root of the sample size and increase in proportion to the distribution D value. However, for data sets that are well sampled over scale ranges >2 orders of magnitude, the confidence limits remain constant and independent of the distribution D value. *Pickering et al.* [1995] synthesized the results of the simulations to produce empirical relationships for D value confidence limits at both the 68% and 95% levels.

Figure 6 shows the fault displacement data distribution for north-south striking faults cutting the Kimmeridge Clay Formation. From the log-scale cumulative frequency plot (Figure 6a) it can be seen that these data do not represent a simple power law distribution. Analyzing the distribution pattern closely, two approximately straight line sections, intersecting at ~ 1 m fault displacement, are identified. These are more clearly resolved on the log-interval graph (Figure 6b) where D values of 0.96, for displacements between 2 and 8 m, and 0.67, for displacements between 0.08 and 0.75 m, are obtained. *Hunsdale and Sanderson* [1998] suggest that the change in scaling displayed by the displacement distribution of small sizes reflects the influence of lithological variation on fault initiation and growth.

Faults identified on the Chirp profile of line 1 (Figure 5) have displacements in the range 0.5-221 m and therefore could be expected to have a similar D value to that of large size faults from the onshore section. This is confirmed on both log-scale cumulative frequency and log-interval graphs for fault data in the offshore area (Figure 7). The distribution pattern shown by fault displacement data from the Chirp profile indicate that this data set exhibits power law behaviour, with a D value of 0.90. This is slightly lower than the D value of 0.96 estimated for faults with displacements >2 m from the same population measured along the adjacent coast (Figure 6b).

The small sample size of only 25 faults and limited scale range over 1 order of magnitude of the onshore data results in large confidence limits [see *Pickering et al.*, 1995] on the estimated D value of 0.96 (±0.2 at the 68% level and ±0.4 at the 95% level). The greater sample number and larger range of fault throw in the offshore data give a narrower confidence interval in the estimated D value of 0.90 (±0.07 at the 68% level and ±0.14 at the 95% level).

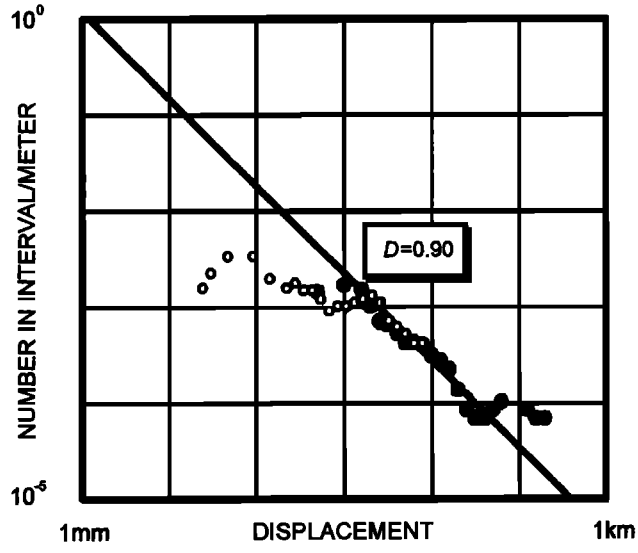

Figure 8. Log-interval graph of fault displacement plotted against number of faults of similar displacement per metre of traverse. The onshore (open circles) and offshore (solid circles) data overlap in the range 1 - 10 m with both data sets having similar densities over this range. The graph also shows that a D value of 0.9 characterises fault displacement over >2 orders of magnitude.

The two data sets thus overlap within confidence limits. Given the greater degree of confidence produced by the larger offshore data set, 0.90 is a more accurate estimate of the true D value for large size faults (throw greater than 1 - 2m).

Direct comparison of data collected in the onshore and marine environment can be done by normalizing the data sets to traverse length [*Jackson and Sanderson*, 1993; *Pickering et al.*, 1994]. Normalizing the data produces a plot of cumulative number per meter (i.e., cumulative fault density) against displacement, thus allowing direct comparison of fault displacement densities from traverses or sections of unequal length. Since the power law nature and change in scaling of onshore faults is more clearly shown on the log-interval graph (Figure 6b), the normalized graph of both data sets is presented in this form (Figure 8). From Figure 8 it can be seen that onshore and offshore fault populations with displacement's >1 m overlap, and both show a power law distribution with a D value of ~ 0.9. Furthermore, the similarity in fault densities in the range 1 - 10 m indicates that all faults with displacement greater than 1 m are resolved on the Chirp profile.

6. Conclusions

The application of Chirp subbottom profiling equipment in the near-shore Weymouth Bay area has allowed detailed imaging of faults with displacements in the range 1 - 200 m and has led to significant advances in the understanding of the distribution characteristics of the north-south striking normal fault set exposed along the adjacent Dorset coast. Advances made and conclusions drawn from this study are summarized below:

1. The Chirp subbottom profiling system can be a useful tool in the geological investigation of near-shore geology and allows the integration of onshore and offshore geology. The profiles presented here demonstrate the level of image quality which can be produced for both high-resolution stratigraphic and structural (fault) studies.

2. Fault displacement data sets rarely contain any meaningful data in the range between the upper limit of outcrop resolution (tens of meters) and below the limit of conventional seismic resolution. This study provides a data set which spans this gap.

3. Data collected in the offshore area demonstrate the fractal nature of fault displacement over 2.5 orders of magnitude (1 - 221 m displacement) with an estimated D value of 0.9. A smaller population of onshore faults, with displacements >1 - 2 m, have a similar D value of 0.96, which is within error of the offshore D value at both the 68% and 95% confidence levels. The integration of fault displacement data, acquired from both outcrop and high-resolution seismic studies, highlight the usefulness of fractal analysis and the importance of field-derived data sets.

Acknowledgments. The authors thank D. Burden, M. Lucas, and N. Richmond for help in data acquisition, D. Emersly and R. J. Quinn for help with data processing, and are grateful to J. McBride, E. J. M Willemse, and G. Yielding for critical reviews. This work was supported by the University of Southampton and NERC grant GR3/9533. R. Hunsdale acknowledges a research studentship from Phillips Petroleum U.K. Ltd.

References

Arkell, W. J., The Portland Beds of the Dorset mainand, *Proc. Geol. Assoc.*, *46*, 301-347, 1935.

Arkell, W. J., The Corallian Beds of Dorset, *Proc. Dorset Nat. Hist. Archaeol. Soc.*, *57*, 59-93, 1936.

Arkell, W. J., The geology of the country around Weymouth, Swanage, Corfe and Lulworth, *Mem. Geol. Surv. G.B.*, *7*, 242-312, 1947.

Bray, R. J., I. R. Ruddy, and P. F. Green, Multiple heating episodes in the Wessex Basin: Implications for geological evolution and hydrocarbon generation, in *Development and Evolution of the Wessex Basin*, edited by J. G. Underhill, *Geol. Soc. Spec. Publ. London*, in press, 1998.

Chadwick, R. A., Permian, Mesozoic, and Cenozoic structural evolution of England and Wales in relation to the principles of extension and inversion tectonics, in *Atlas of Onshore Sedimentary Basins in England and Wales: Post Carboniferous Tectonics Stratigraphy*, edited by A. Whittaker, pp. 9-25, Blackie, Acad. and Prof. New York, 1985.

Chadwick, R. A., Aspects of basin inversion in southern Britain, *J. Geol. Soc. London*, *150*, 311-322, 1993.

Childs, C., J. J. Walsh, and J. Watterson, A method for estimation of the density of fault displacements below the limits of seismic resolution in reservoir formations, in: *North Sea Oil and Gas Reservoirs II*, pp. 309-318, edited by A. T. Buller, Graham and Trotman, Norwell, Mass., 1990.

Coward, M. P., and D. Dietrich, Alpine tectonics; An overview, in *Alpine Tectonics*, edited by M. P. Coward, D. Dietrich, and R. G. Park, *Geol. Soc. Spec. Publ. London*, *45*, 1-29, 1989.

Cox, B. M., and R. W. Gallois, The stratigraphy of the Kimmeridge Clay of the Dorset type area and its correlation with some other Kimmeridgian sequences, *Rep. 80/4, Inst. of Geol. Sci.*, London, Eng., U.K., 1981.

Curry, D., The Palaeogene Beds of south-east England, *Proc. Geol. Assoc.*, *76*, 151-173, 1965.

Donovan, D. T., and A. H. Stride, An acoustic survey of the sea floor south of Dorset and its geological interpretation, *Philos. Trans. R. Soc. London*, *44*, 299-330, 1961.

Drummond, P. V. O., The mid-Dorset Swell: Evidence of Albian-Cennomanian movements in Wessex, *Proc. Geol. Assoc.*, *81*, 679-714, 1970.

El-Shahat, A., and I. M. West, Early and late lithification of aragonite bivalve beds in the Purbeck Formation (Upper Jurassic-Lower Cretaceous), southern England, *Sediment. Geol.*, *35*, 15-41, 1981.

Ensom, P. C., An annotated section of the Purbeck Limestone Formation at Worbarrow Tout, Dorset, *Proc. Dorset Nat. Hist. Archaeol. Soc.*, *106*, 87-91, 1985.

House, M. R., The structure of the Weymouth Anticline, *Proc. Geol. Assoc.*, *71*, 221-238, 1961.

House, M. R., Geology of the Dorset Coast, in *Geologists' Association Guide*, 2nd ed., edited by C. J. Lister, pp. 33-36, 107-132, Holywell, Oxford, Eng., U.K., 1989.

Hunsdale, R., and D. J. Sanderson, Fault distribution analysis, an example from Kimmeridge Bay, Dorset, U.K., in *Development and Evolution of the Wessex Basin*, edited by J. G. Underhill, *Geol. Soc. Spec. Publ. London*, *133*, 299-310, 1998.

Jackson, P., and D. J. Sanderson, Scaling of fault displacements from the Badajoz-Cordoba shear zone, SW Spain, *Tectonophysics*, *210*, 179-190, 1992.

Kakimi, T., Magnitude-frequency relation for displacement of minor faults and its significance in crustal deformation, *Bull. Geol. Surv. Jpn.*, *31*, 486-487, 1980.

Karner G. D., S. D. Lake, and J. F. Dewey, The thermo-mechanical development of the Wessex Basin, southern England, in *Continental Extension Tectonics*, edited by P.L. Hancock, J. F. Dewey, and M. P. Coward, *Geol. Soc. Spec. Publ. London*, *28*, 517-536, 1987.

Lake, S. D., and G. D. Karner, The structure and evolution of the Wessex Basin, southern England: an example of inversion tectonics, *Tectonophysics*, *137*, 347-378, 1987.

La Pointe, P. R., and J. A. Hudson, Characterisation and interpretation of Rock Mass Joint Patterns, *Geol. Soc. Am. Spec. Pap.*, *199*, 37, 1985.

Marrett, R., Aggregate properties of fracture populations, *J. Struct. Geol.*, *18*, 169-178, 1996.

Marrett, R., and R. W. Almendinger, Estimates of strain due to brittle faulting: Sampling of fault populations, *J. Struct. Geol.*, *13*, 735-738, 1991.

Needham, T., G. Yielding, and R. Fox, Fault population description and prediction using examples from the offshore U.K., *J. Struct. Geol.*, *18*, 155-167, 1996.

Peacock, D. C. P., and D. J. Sanderson, Strain and scaling of faults in the chalk at Flamborough Head, U.K., *J. Struct. Geol.*, *16*, 97-107, 1994.

Penn, I. E., R. A. Chadwick, S. Holloway, G. Roberts, T. C. Pharaoh, J. M. Allsop, A. G. Hulbert, and I. M. Burns, Principal features of the hydro carbon prospectivity of the Wessex-Channel Basin, U.K., in *Petroleum Geology of North West Europe*, edited by J. Brooks and K. Glennie, pp.139-148, Graham and Trotman, Norwell, Mass., 1987.

Pickering G., J. M. Bull, D. J. Sanderson, and P. V. Harrison, Fractal fault

displacements: A case study from the Moray Firth, Scotland, in *Fractals and Dynamic Systems in Geosciences*, edited by J. H. Kruhl, pp.105-119, Springer-Verlag, New York, 1994.

Pickering G., J. M. Bull, and D. J. Sanderson, Sampling power law distributions, *Tectonophysics*, *248*, 1-20, 1995.

Press, W. H., B. P. Flannery, S. A. Teukolsky, and W. T. Vetterling, *Numerical Recipes: The Art of Scientific Computing*, Cambridge Univ. Press, New York, 1986.

Scholz, C. H., and P. A. Cowie, Determination of total strain from faulting using slip measurements, *Nature*, *346*, 837-839, 1990.

Selley, R. C., and R. Stoneley, Petroleum habit in south Dorset, *in Petroleum Geology of North West Europe*, edited by J. Brooks and K. Glennie, pp.139-148, Graham and Trotman, Norwell, Mass., 1987.

Sun, S. Q., Facies-related diagenesis in a cyclic shallow marine sequence: The Corallian Group (Upper Jurassic) of the Dorset coast, southern England, *J. Sediment. Petrol.*, *60*, 42-52, 1990.

Talbot, M. R., Major sedimentary cycles in the Corallian Beds (Oxfordian) of southern England, *Palaeogeogr. Palaeoclimatol. Palaeoecol.*, *14*, 293-317, 1973.

Talbot, M. R., Ironstones in the Upper Oxfordian of southern England, *Sedimentology*, *21*, 433-450, 1974.

Townson, W. G, Geology of the Coombe Valley, *Proc. Dorset Nat. Hist. Archaeol. Soc.*, *95*, 7-18, 1975.

Walsh, J. J., J. Watterson, and G. Yielding, The importance of small-scale faulting in regional extension, *Nature*, *351*, 391-393, 1991.

Wilson, R. C. L., Diagenetic carbonate fabric variations Jurassic limestones in southern England, *Proc. Geol. Assoc.*, *78*, 535-554, 1967.

Wilson, R. C. L., Carbonate facies variations in the Osmington Oolite Series in southern England, *Palaeogeogr. Palaeoclimatol. Palaeoecol.*, *4*, 258-281, 1968.

Wright, J. K., A new look at the stratigraphy, sedimentology and ammonite fauna of the Corallian Group (Oxfordian) of South Dorset, *Proc. Geol. Assoc.*, *97*, 221-228, 1986.

Yielding, G., J. J. Walsh, and J. Watterson. The prediction of small-scale faulting in reservoirs, *First Break*, *10*, 449-460, 1992.

Ziegler, P. A., Late Cretaceous and Cenozoic intra-plate compressional deformations in the Alpine foreland: A geodynamic model, *Tectonophysics*, *137*, 389-420,1987.

J. M. Bull, J. K. Dix, and D. J. Sanderson, Department of Earth and Oceanographic Sciences, University of Southampton, Southampton Oceanographic Centre, Empress Dock, European Way, Southampton SO14 3ZH, England, U. K. (e-mail: djs2@soc.soton.ac.uk)

R. Hunsdale, Phillips Petroleum Company Norway, P.O. Box 220, Tananger, N-4056 Norway. (e-mail: rhunsda@bvemx.ppco.com)

(Received March 19, 1997; revised August 5, 1997;
accepted December 15, 1997.)